Long-Term Analysis of Temperature and Current-Dependent Degradation in Green High-Power Light-Emitting Diodes

Herzog, Alexander; Buffolo, Matteo; Piva, Francesco; Benkner, Simon; Zandi, Babak; Balasus, Jens; Myland, Paul; Wirth, Felix; Van Driel, Willem D.; Meneghini, Matteo

DOI
10.1109/ACCESS.2025.3599797

Publication date
2025

Document Version
Final published version

Published in
IEEE Access

IEEE Access
Multidisciplinary ⋮ Rapid Review ⋮ Open Access Journal

Received 30 July 2025, accepted 14 August 2025, date of publication 18 August 2025, date of current version 22 August 2025.

Digital Object Identifier 10.1109/ACCESS.2025.3599797

RESEARCH ARTICLE

Long-Term Analysis of Temperature and Current-Dependent Degradation in Green High-Power Light-Emitting Diodes

ALEXANDER HERZOG[1], (Senior Member, IEEE), MATTEO BUFFOLO[2], (Senior Member, IEEE), FRANCESCO PIVA[2], SIMON BENKNER[1,3], BABAK ZANDI[1], JENS BALASUS[1], PAUL MYLAND[1], FELIX WIRTH[1], WILLEM D. VAN DRIEL[4,5], MATTEO MENEGHINI[2,6], (Fellow, IEEE), AND TRAN QUOC KHANH[1]

[1]Laboratory of Adaptive Lighting Systems and Visual Processing, Technische Universit'at Darmstadt, 64289 Darmstadt, Germany
[2]Department of Information Engineering, University of Padova, 35131 Padua, Italy
[3]klion GmbH, 64295 Darmstadt, Germany
[4]Electronic Components, Technology and Materials (ECTM), Department of Microelectronics, Delft University of Technology, 2628 CD Delft, The Netherlands
[5]Signify, 5656 AE Eindhoven, The Netherlands
[6]Department of Physics and Astronomy, University of Padova, 35131 Padua, Italy

Corresponding author: Alexander Herzog (herzog@lichttechnik.tu-darmstadt.de)

This work was supported by the Electronics Components and Systems for European Leadership (ECSEL) Joint Undertaking (JU) under Grant 101007319.

ABSTRACT We report on the degradation dynamics and mechanisms of commercially available green high-power light-emitting diodes (LEDs) with a peak wavelength of 522 nm. The stress tests were carried out for up to 8800 hours with forward currents ranging from 350 mA to 1000 mA at junction temperatures between 86 °C and 155 °C. Two complementary test designs were used to isolate temperature- and current-driven effects. The results of the accelerated tests reveal the following key findings: 1.) A square-root–time-dependent loss in the quantum wells caused by the generation of point defects, leading to up to 90 % flux reduction within the first 500 hours at low forward currents. 2.) A logarithmic decay governed by defect-induced carrier-injection loss, evident above $I_{\mathrm{EQE,max}}$ and accompanied by a spectral red shift. 3.) A temperature-activated blue shift with an activation energy of $E_{\mathrm{a}} = 0.23$ eV, indicating the coexistence of competing degradation mechanisms. The interplay between different mechanisms results in an enhanced device lifetime at higher stress temperatures and stands in contrast to previous findings reported in the literature. 4.) The isothermal stress test indicates a cubic acceleration of degradation with carrier density, implicating Auger-Meitner-generated hot electrons in defect formation. These insights provide guidance for mitigating reliability issues of green high-power LEDs in future devices.

INDEX TERMS Light-emitting diode (LED), InGaN, high-power LED, reliability, accelerated stress test, green LEDs, green gap.

I. INTRODUCTION

The development of GaN-based LEDs and emitters has been steadily carried forward in recent decades. Especially InGaN emitters in the blue spectral range have been the subject of intensive research, due to the relevance for white light sources in general lighting applications [1], [2]. Nevertheless, the development of GaN emitters outside the blue spectral range has become more prominent. In particular, the peripheral regions of the InGaN material system, which are located in the ultraviolet and green spectral range. These ranges present new technological challenges and offer potential optimizations compared to emitters in the blue spectral range [3], [4], [5], [6]. Despite the technological developments in recent years, green InGaN emitters suffer from reduced efficiency with increasing indium content and the associated

The associate editor coordinating the review of this manuscript and approving it for publication was Jiajie Fan.

increased wavelength. Different lattice constants of InN and GaN result in lattice mismatch occurring in the c-plane and thus promote the formation of piezoelectric effects [7]. The resulting internal pyro- and piezoelectric fields contribute to a separation of the wave functions, reducing the overlap of the functions and thus the probability of radiative recombination [8]. The Coulomb interaction of the separated carriers results in a red-shift of the emission spectrum and the phenomenon is also known as the quantum-confined Stark effect (QCSE). Furthermore, the efficiency of green InGaN-based LEDs is reduced by a higher number of defects, which can be attributed to the previously described lattice mismatch of indium-rich semiconductor structures [9]. Besides the previously described challenges, green InGaN LEDs exhibit a strong efficiency-droop, additionally reducing the efficiency in the range of typically used forward currents of high-power LEDs (350 mA-1000 mA) [10]. Similarly to green InGaN emitters, the efficiency of AlGaInP-based LEDs drops significantly in the green spectral range and even below the efficiency of InGaN-based emitters [11]. Due to the lack of efficient semiconductor emitters in the green spectral range the problem is also referred to as ''green gap''. Approaches to overcome the ''green gap'' by phosphor converted LEDs involves additional drawbacks and problems arising from the broadband emission of the green phosphors and their degradation behavior, which is more difficult to estimate [12], [13].

Even though green LEDs suffer from reduced efficiency, their reliability and lifetime issues are of decisive importance for their use in practical applications. In contrast to the extensive number of publications addressing the degradation mechanisms and dynamics of phosphor-converted white LEDs for general lighting applications, stress tests on green InGaN high-power LEDs have only been published to a limited extent.

According to Li et al., the higher defect density of the indium-rich structures affects the degradation behavior of 530 nm emitters [14]. Their results indicated a decrease in radiant flux by 5 % within 1000 hours of operation for a stress current of 20 mA. The results published by Renso et al. indicated up to 20 % optical power loss in semiconductor structures with a peak emission wavelength of 550 nm. Stress tests performed at high-power operating currents (350 mA) indicated a 2 % radiant flux depreciation after 2000 hours of operation in 530 nm LEDs [15].

Independent of the detailed device characteristics, the aforementioned studies attribute the optical power loss to the formation of point defects, the causality of which is not specified in detail. The formation of point defects in green InGaN LEDs is manifested by Meneghini et al. [16]. Operating the devices in reverse bias at −25 V induced significant changes in the current-voltage characteristics accompanied by radiant flux depreciation.

Further, the data of accelerated degradation tests indicate processes of electromigration with increasing current density [4]. As a result, the local resistance of the semiconductor structures varies and reduces the electro-optical efficiency of the device. Miller et al. [17] demonstrated the degradation of electrical contacts in comparable experimental conditions.

In conclusion, the existing literature gives sparse information about green InGaN degradation dynamics and mechanisms. The effect of the different operating conditions on the degradation behavior is not addressed in the published literature, even though information about temperature and current dependent degradation is of great interest if multi-channel luminaires with colorimetric stability should be designed.

To address the knowledge gap regarding the long-term stability of indium-rich quantum well structures and the dependencies of underlying degradation mechanisms, 520 nm emitters are characterized and analyzed within the scope of this paper. Section III discusses general degradation mechanisms and characteristics of the stressed devices, whereas temperature and current-driven effects are separated in Sections IV and V.

II. EXPERIMENTAL DETAILS

A. SAMPLES

The long-term experiments were carried out on commercially available green high-power LEDs with a peak wavelength of 522 nm measured at a forward current of $I_f = 350$ mA. The maximum external quantum efficiency (EQE) could be quantified with $EQE_{max} = 42\,\%$ and is located in the range of forwards currents between $I_f = 1$ mA and 7 mA. Due the strong efficiency droop of the emitters, the external quantum efficiency reduces to $EQE = 19\,\%$ at a 2x nominal current of $I_f = 700$ mA. Therefore, an efficiency droop of $1 - \eta_{EQE,700mA}/\eta_{EQE,max} = 55\,\%$ can be determined on average. Typical characteristics of the analyzed samples are listed in Table 1.

TABLE 1. Overview of initial device characteristics measured at the nominal current of $I_f = 350$ mA and $T_c = 25°C$. The values given are mean values with associated standard deviations.

Number of samples n	Peak-wavelength (nm)	Optical power (mW)	Forward voltage (hours)	Electrical power (W)
24	522, 4 ±1.2	191.4 ±3.7	3.382 ±0.036	1.185 ±0.013

The green high-power emitters are mounted in 3535 ceramic SMD packages with a silicone encapsulation lens. For the aging tests performed, each LED was assembled on a metal core printed circuit boards (MCPCBs). Next to the LEDs solder point a temperature sensor (PT100) was placed, allowing to control the solder point temperature during measurement and during stress test. The stress tests were performed on temperature-controlled heating plates. Since no temperature chambers were used, the ambient temperature of the stress test can be quantified with $T_a = 25\,°C$ at a relative humidity of $RH = 30\,\%$. Irrespectively of the selected stress test conditions, four LEDs each were operated at the same stress condition.

TABLE 2. Selected test conditions for the performed aging test. Junction temperatures were calculated with the determined thermal resistance.

Stress current I_a (mA)	Junction temperature $T_j \pm 4$ K (°C)	Stress time t (hours)
350	135	7500
700	86, 116, 135, 155	8803
1000	135	7500

To analyze the current- and temperature-induced degradation dynamics of the emitters, two different test designs were selected, each with a minimum testing duration of 6000 hours, as recommended by the LM-80-20 standard [18]. The temperature dependent degradation was analyzed for a test period of 8800 hours and the devices were operated at four different temperatures, inspired by typical LM-80-20 standard test conditions ($T_c = 55$ °C and 85 °C) and extended conditions (105 °C and 125 °C) [18]. Throughout the test, a constant stress current of $I_a = 700$ mA was applied, corresponding to twice the rated nominal current. The different case temperatures were achieved by controlling heating plates in combination with the previously mentioned temperature sensors. To assess the LEDs' junction temperatures, the thermal resistances were measured using a thermal impedance measurement system (T3ster - Mentor Graphics). For the analyzed samples a thermal resistance of $R_{th} = 14.7\,\mathrm{K\,W^{-1}}$ was determined on average, resulting in the stress test conditions shown in Table 2.

The current-induced degradation dynamics was analyzed using an isothermal stress test and was carried out for a period of 7500 hours. Taking into account the measured thermal resistance, the devices were operated at a junction temperature of approximately $T_j = 135$ °C and three different aging currents $I_a = 350$ mA, 700 mA and 1000 mA. The stress currents were selected at the rated nominal current (350 mA), at twice the nominal current (700 mA) and at the absolute maximum rating (1000 mA). The estimation of the temperature with an uncertainty of ±4 K results as a worst-case estimate. The determination of T_j is affected by the measurement of the thermal resistance, the absolute radiant flux and the temperature coefficient k. Consequently, the uncertainty is to be considered as an expanded measurement uncertainty ($P = 95.4$ %). The selected aging conditions, as listed in Table 2, were knowingly chosen within and above the maximum junction temperature specified by the manufacturer ($T_{j,max} = 125$ °C) to deliberately provoke and accelerate degradation mechanisms within a reasonable timeframe.

During the stress tests, the optical and electrical characterization of the devices was performed in non-equidistant intervals to capture the initially stronger degradation rate with a reasonable temporal resolution. For each measurement, the LEDs were disassembled from the heating plates and measured at a dedicated LED measurement system. The optical measurements were carried out using a 30 cm-integrating sphere with 2π-geometry in combination with a spectroradiometer (CAS140CT - Instrument Systems). The LED-mount integrated peltier element was controlled by a peltier controller (ITC4020 - Thorlabs) and was used to stabilize the LED's case temperature during the characterization at $T_c = 25$ °C. Measurements at forward currents above 1 mA were carried out as pulsed measurements, allowing to reduce joule-heating within the active region. For these measurements the integration time of the spectroradiometer was set to 10 ms, with a current pulse width of 15 ms. Due to the fact that a pulsed current of 15 ms could cause effects of joule-heating, the integration time and pulse width was kept constant for the entire stress test period allowing to assume a systematic error in radiant flux. To study the efficiency droop with increasing stress time, the spectrum was taken at 16 different forward currents (100 µA, …, 700 mA). Additionally, the I-V characteristic was recorded at each measurement interval, using a source measure unit (Keithley 2450).

III. DEGRADATION MECHANISMS

A. REPRESENTATIVE DEVICE CHARACTERISTICS

Before analyzing the effect of stress temperature and stress current on radiant flux depreciation, the occurring aging mechanisms are described in a representative manner using the measurement data from a single device. Fig. 1 shows the decrease in normalized radiant flux for an aging current of $I_a = 700$ mA and a stress test case temperature of $T_c = 55$ °C ($T_j = 86$ °C). Data over 8800 hours of stress are presented for different measurement currents I_m and indicate an operating-point-dependent effect of the degradation mechanisms. The operating range below 30 mA shows a significant reduction in radiant flux, resulting in an optical power loss of up to 90 % for a measurement current of 100 µA. In contrast, the extent of optical degradation for a measurement current of $I_m = 350$ mA is comparatively small and can be quantified with an optical power loss of 10 %. Regardless of the operating point considered, the decrease in radiant flux occurs

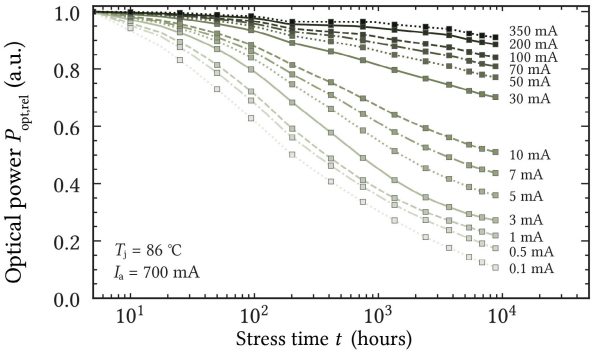

FIGURE 1. Reduction of optical power $P_{opt,rel}$ for different measurement currents I_m (normalized to the value at 0 h) for a period of 8800 hours. The degradation dynamics are representative for devices operated at a stress temperature of $T_j = 86$°C and stress current of $I_a = 700$ mA. The device was measured at a case temperature of $T_c = 25$°C.

primarily within the first 2000 hours of operation, followed by a significantly smaller degradation rate between 2000 and 8800 hours.

Analogously to the measurement data presented above, the reduction in external quantum efficiency for different forward currents is shown in Fig. 2. Below the efficiency maximum, located at approximately $I_{\mathrm{EQE,max}} = 3\,\mathrm{mA}$ before stress, a significant decrease in efficiency is observed, which is much less pronounced above $I_{\mathrm{EQE,max}}$ and continues to diminish with increasing forward current. Besides the strong impact of the degradation mechanisms on the range below the efficiency maximum, the efficiency maximum gradually shifts to higher forward currents over stress time. The corresponding efficiency droop, defined by

$$\mathrm{Droop} = 1 - (\eta_{\mathrm{EQE,max}}/\eta_{\mathrm{EQE,700mA}}) \cdot 100\% \,, \quad (1)$$

decreases from 55 % before stress to 30 %, whereas $I_{\mathrm{EQE,max}}$ increases from 3 mA to 50 mA over 8800 hours of operation.

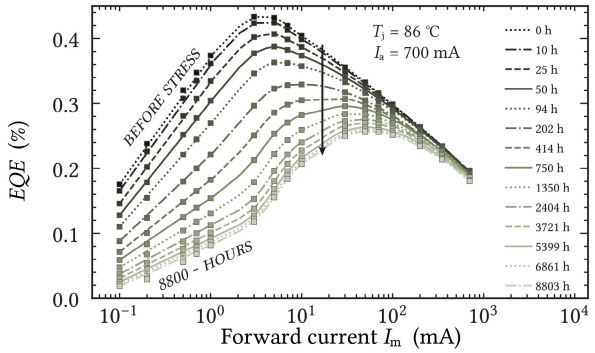

FIGURE 2. Current-dependent external quantum efficiency (*EQE*) for a stress period of 8800 hours. The degradation dynamics are representative for devices stressed at $T_j = 86°C$ and a current of $I_a = 700$ mA. The device was measured at a case temperature of $T_c = 25°C$.

The gradual power loss is accompanied by a steeper slope in the log-log *L-I* curves, shown in Fig. 3. In the region of the efficiency maximum EQE_{max} the slope p of the logarithmic *L-I* curves can be quantified with $p \approx 1$, indicating the dominance of radiative recombinations at these operating points [2].

Forward currents below EQE_{max} are primarily affected by non-radiative recombination contributions, indicated by values $p > 1$, whereas forward currents at $I_m > I_{\mathrm{EQE,max}}$ are driven by non-radiative recombination events arising from carrier-overflow or Auger-Meitner-recombination (AM), represented by values of $p < 1$ [2]. During 8800 hours of stress, the efficiency maximum shifts from $I_{\mathrm{EQE,max}} = 3\,\mathrm{mA}$ to 50 mA and thus the logarithmic *L-I* slope with $p \approx 1$. For the operating point at $I_m = 100\,\mu\mathrm{A}$ the slope p increases from 1.44 to 1.64, whereas at $I_m = 200\,\mathrm{mA}$ a slight increase from 0.8 to 0.85 can be observed. Due to a balance shift of SRH and radiative recombination, the proportion of SRH recombination is smaller with increasing forward current.

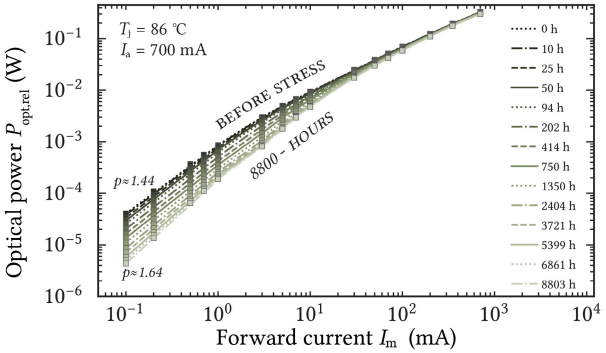

FIGURE 3. Log-Log *L-I* plot for 8800 hours of stress, with calculated slope *p* of the logarithmic *L-I* curves. The degradation dynamics are representative for devices operated at $T_j = 86°C$ and stress current of $I_a = 700$ mA. The characteristics were measured at a case temperature of $T_c = 25°C$.

Apart from the radiant flux depreciation, the electrical characteristics are analyzed within the scope of this work. The semi-logarithmic *I-V* characteristics shown in Fig. 4 reveal a pronounced increase in conductivity within the low-injection regime over the 8800-hour stress period. At a forward current of $I_f = 1\,\mathrm{nA}$ for example, the corresponding forward voltage V_f drops from initially 1.6 V to 0.1 V after stress. This substantial voltage drop indicates the formation of parasitic conductive paths that bypass the active region. At higher forward currents in the high-injection regime, the voltage reduction is less pronounced and becomes only marginally noticeable.

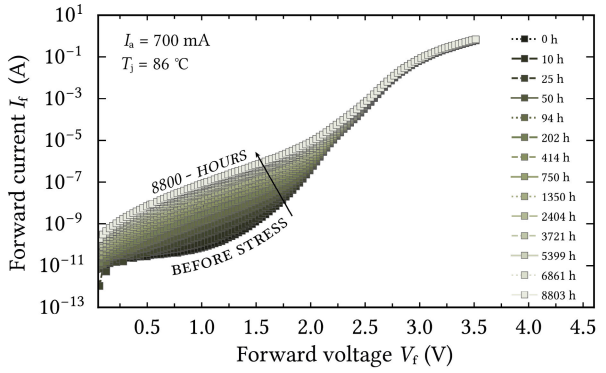

FIGURE 4. Semi-logarithmic *I-V* characteristics of one representative sample stressed at a junction temperature of $T_j = 86°C$ and a forward current of $I_a = 700$ mA for 8800 hours of stress. The device was characterized at a case temperature of $T_c = 25°C$.

The differential series resistance is derived from the *I-V* characteristics and its depreciation for the entire stress test period is shown in Fig. 5. The initial series resistance $R_s = 0.57\,\Omega$ decreases by 10.5 % to $R_s = 0.51\,\Omega$.

For an operation time of $t > 200$ h a square-root-time dependence can be identified. Taking into account the time dependence of the determined ideality factor n_{ideal}, inferred from the measurement data using the method described by [19], an analogous behavior can be identified. Therefore,

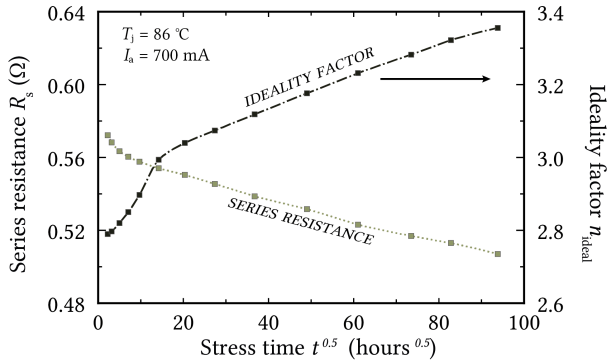

FIGURE 5. Square-root-time-dependet differential series resistance R_s and ideality factor n_{ideal} for 8800 hours of stress. The degradation dynamics are representative for devices operated at $T_j = 86°C$ and stress current of $I_a = 700$ mA. The measurement was taken at a case temperature of $T_c = 25°C$.

n_{ideal} increases within the first 200 hours of operation from 2.79 to 2.99 and continues gradually following a square-root–time dependence to 3.36.

The decrease in optical power is accompanied by changes in the spectral characteristics, which can be quantified by shifts in the peak wavelengths $\Delta_{\lambda,peak}$. Due to an operating-point-dependent shift in peak wavelength and radiant flux depreciation, three representative operating points are selected and analyzed according to Fig. 6.

For measurement currents below 3 mA, a blue shift of up to $\Delta_{\lambda,peak,100uA} = 1.2$ nm can be observed, whereas between 3 mA and 700 mA a red shift with a maximum of $\Delta_{\lambda,peak,10mA} = 1.2$ nm occurs. For measurement currents above 200 mA, the red shifts are below 0.6 nm. The optical power loss for $I_m = 100$ µA indicates a square-root-time dependence within the first 200 hours of operation. Subsequent degradation dynamics for time steps $t > 200h$ can be described by a logarithmic decay function and are therefore missing a correlation with the square-root-time-dependent blue shift of the peak wavelength.

The radiant flux decay for the operating range between $I_{EQE,max} = 3$ mA and 200 mA is represented by the data measured at $I_m = 10$ mA. A detailed analysis of the data reveals an analogous behavior compared to the operating point at $I_m = 100$ µA. In contrast to operating points below $I_{EQE,max}$, the initial square-root-time dependence superimposes effects of the competing logarithmic dynamics to a higher degree. Nevertheless, the subsequent flux decay is dominated by a logarithmic progression for operating points between the efficiency maximum and 200 mA.

Due to the logarithmic time dependence of the spectral (λ_{peak}) and integral ($P_{opt,rel}$) characteristics for $t > 200$ h, a linear correlation between radiant flux decay and the red shift of the peak wavelength is observed in this operating range. Operating points close to the nominal current of 700 mA indicate two superimposed degradation processes with a square-root-time dependence, here representatively shown by the results measured at $I_m = 200$ mA. The initial drop for $t \leq 200$ h shows a stronger degradation rate compared to the subsequent stress time. In contrast to the flux depreciation, the spectral red shift follows a logarithmic time dependence.

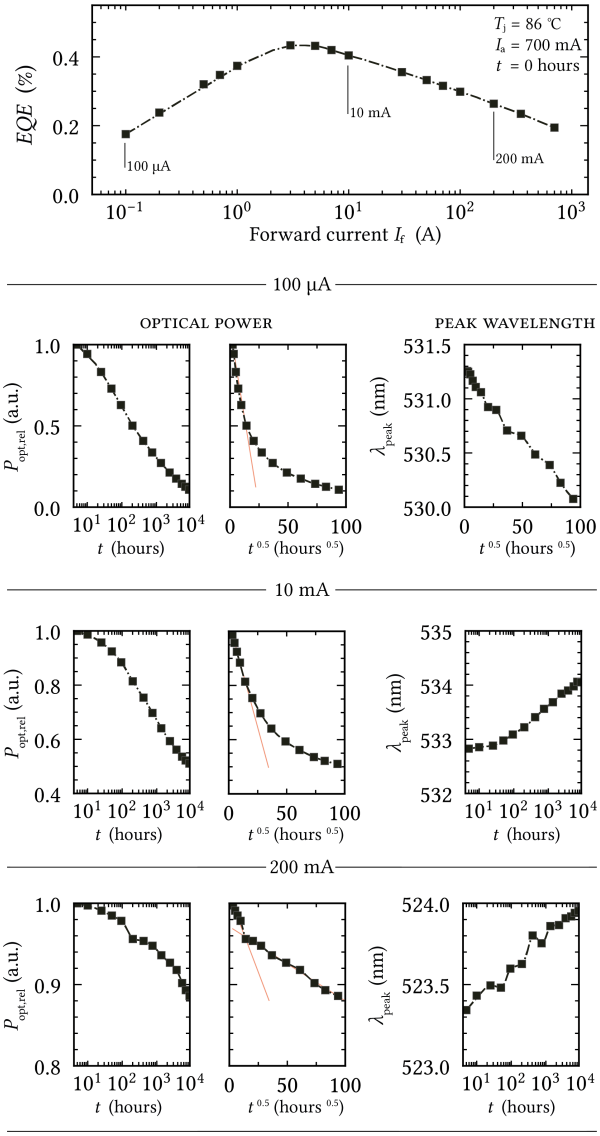

FIGURE 6. Representative operating points 100 µA, 10 mA, 200 mA highlighted in the current-dependent *EQE* plot. Radiant flux decay and peak wavelength shift over the operating period for 100 µA, 10 mA, 200 mA. The degradation dynamics are representative for devices operated at $T_j = 86°C$ and stress current of $I_a = 700$ Ma. The characterization was carried out at a case temperature of $T_c = 25°C$.

To exclude additional effects induced by a thermal interface degradation, the thermal structure functions of the devices were measured before and after 8800 hours of stress (not shown here). For the aging period considered, no changes in the thermal structure functions can be identified. Therefore it can be concluded that the previously described spectral shifts are not caused by degradation mechanisms of the thermal interface.

B. DISCUSSION OF DEGRADATION MECHANISMS

The results presented in Figure 1 indicate an operating-point-dependent radiant flux depreciation. The effect can be

attributed in part to trap-assisted tunneling processes (TAT) and primarily to the generation of non-radiative recombination centers [20]. Taking into account the I-V characteristics, shown in Fig. 4, the generation of the point defects in and around the active region can be confirmed, since the electrical characteristics indicate a significant forward current increase in the low-injection regime [21], [22], [23]. According to Roccato et al., an increase in leakage current is due to energetically favorable conductive paths arising from generated mid-gap states, resulting in trap-assisted tunneling processes bypassing the active region [24], [25]. The higher conductivity of the leakage path contributes to a voltage drop varying in magnitude as a function of forward current. Furthermore, the increasing slope p presented in the log-log L-I plot in Fig. 3 manifests an increased number of non-radiative recombination centers (NRRCs) favoring Shockley-Read-Hall (SRH) recombination [2]. These NRRCs primarily affect the efficiency of the devices at low current levels. As the defects become saturated with higher current density, their effect on flux depreciation declines [25].

A closer analysis of the data reveals not only varying levels of radiant flux depreciation for the individual operating points, but also different degradation dynamics depending on the applied forward current. An operating point of 100 µA shows an almost continuous logarithmic optical power decay, whereas the dynamics for operating points between $I_{\mathrm{EQE,max}}$ and 200 mA can be separated in two degradation modes $m1$ and $m2$.

Mode $m1$ can be defined for a stress period $t < 200$ h, indicating a square-root-time dependence of the optical power decay. For time steps $t \geq 200$ h mode $m1$ is subsequently changing to mode $m2$ with a logarithmic decay characteristic. Operating points above 200 mA exhibit a square-root-time dependence for both mode $m1$ and mode $m2$.

To analyze the complex interaction of different degradation mechanisms in depth, the peak wavelengths shifts shown in Figure 6 and their accompanying decrease in optical power are discussed in detail.

The blue shift of the peak wavelength, which can be observed for operating points below the efficiency maximum $I_{\mathrm{m}} \ll I_{\mathrm{EQE,max}}$, can be attributed to a reduced localization of carriers in indium-rich regions of the quantum wells [26]. These localization centers are due to manufacturing-induced variations in indium content, preventing recombination of carriers across defects. Due to the energetically favorable states, carriers concentrate in these regions of the quantum wells and recombine predominantly radiatively. The increase of point defects in the quantum well region reduces the carrier diffusion length and thus increases the probability of non-radiative recombinations. As a result, the occupation probability of energetically lower localization states is reduced and the radiative recombination in band-edge levels and localization states is suppressed, as shown schematically in Fig. 7 [26], [27], [28].

Previous studies [26], [29], [30] have indicated that the full width at half maximum (FWHM) is affected

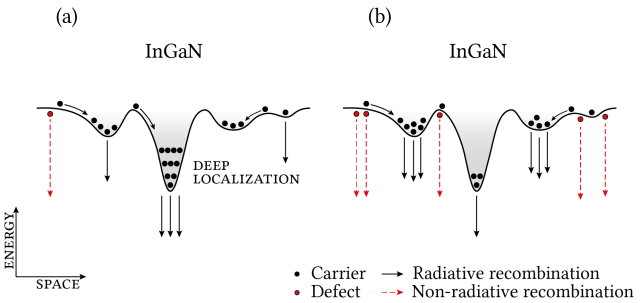

FIGURE 7. Schematic illustration of localized carriers recombining primarily in indium-rich regions (a.). Carrier recombination close to the band gap region due to a reduced occupation probability of energetically lower localization states (b).

by nanometer-scale potential fluctuations, which serve as localization centers and modify the low-energy portion of the spectrum. Compared to blue-emitting MQWs, green-emitting MQWs exhibit deeper localization states, primarily due to significant phase separation and indium segregation in the indium-rich regions [26], [31]. Thus, particularly in the low-injection region where carriers are susceptible to point defects, the diminishing localization effect can also be observed through the reduction of the low-energy wing in the aged spectrum and a blue shift of the emitted peak wavelength. The previously described interactions can be manifested by the results shown in Fig. 6, which indicate a significant blue shift of the peak emission wavelength. Furthermore, a reduction of up to 1.2 nm in FWHM was observed depending on stress condition ($T_{\mathrm{j}} = 155\,^{\circ}\mathrm{C}$).

The progression of the blue shift follows a square-root-time dependence for the entire stress test period, as shown in Fig. 6, whereas the decrease in optical power can be described by two separated degradation modes $m1$ and $m2$. Consequently, the radiant flux decay and the peak wavelength shift can be linked to competing degradation mechanisms.

Radiatively recombining carriers within the quantum wells are determining the emitted spectrum of the device and are thus primarily affected by an increase in non-radiative recombination centers within the quantum wells. Accordingly, the increase of these NRRCs follows a square-root-time dependence, which is reflected in the optical power depreciation of the device during mode $m1$.

Furthermore, the radiant flux is affected by the number of carriers being injected into the quantum wells [32]. Due to additional defects in the active region, energetically favorable conductive paths are bypassing the quantum well region. As a consequence, the reduced proportion of carriers being injected into the quantum wells affects the radiative recombination rate R_{Rad} of the device. The accumulation of these defects follows a logarithmic time dependence, superimposing and dominating the degradation dynamics of the considered operating range for time steps $t > 200$ hours ($m2$). As a result, two different degradation dynamics can be observed for the radiant flux depreciation and its spectral shift.

For operating points above $I_{EQE,max}$ (e.g. 10 mA) the optical degradation is accompanied by a red shift of the emission spectrum. Analogously to the previously presented results, the flux depreciation can be assigned to two different mechanisms allowing the characteristics to be divided into two separate modes. The initial square-root decrease in radiant flux is progressively superimposed by the logarithmic progression of bypassing conductive paths. The square-root-time-dependent degradation for $t < 200$ h is reflected in the radiant flux depreciation, but the expected associated blue shift is not discernible due to the superimposition of a simultaneous occurring red shift. For a stress time $t \geq 200$ h, a linear correlation between the radiant flux decay and the spectral red shift is observed.

The occurring red shift results from a reduced screening of internal polarization fields in the quantum well region. Since indium-rich InGaN layers show a significant lattice mismatch to surrounding GaN barriers, the induced lattice strain results in internal polarization fields and thus in a reduced electron–hole wave function overlap, also known as quantum-confined stark effect (QCSE) [33], [34]. An initial characterization of the devices revealed a blue shift of the peak wavelength with increasing pulsed forward current. According to Renso et al., this behavior can be attributed to a compensation of the internal polarization fields with increasing carrier density [4]. It is therefore reasonable to assume a significant QCSE for the analyzed devices, as commonly observed for green InGaN emitters [34].

Taking these factors into consideration, the time-dependent generation of point defects and the previously described energetically favorable parasitic conductive paths, decrease the number of carriers being injected into the quantum well region. Consequently, the dominance of Auger-Meitner processes or an overflow of charge carriers occurs at higher injection levels compared to the pristine state of the device, resulting in a shift of the efficiency maximum $I_{EQE,max}$ as shown in Fig. 2. Simultaneously, fewer carriers are contributing to the compensation of the internal electrical fields within the quantum wells, thus inducing the observed red shift of the peak wavelength, schematically shown in Fig. 8.

For operating points > 200 mA, the recombination mechanisms before stress are dominated primarily by non-radiative AM processes [35]. In this operating range, the carrier density is only insignificantly reduced by the increase of TAT processes and NRRCs, which is linked to comparatively slight changes in the emission spectrum. The spectral changes indicate a continuous logarithmic characteristic, whereas the decrease in radiant flux shows a square-root–time dependence for the two degradation modes $m1$ and $m2$. Accordingly, mechanisms occurring within the saturated QWs prevail for these operating points, which can be manifested by the square-root increase of the ideality factors.

In conclusion, it can be stated that two different mechanisms primarily contribute to the degradation of the device. The mechanism occurring within the first 200 hours of operation exhibits a square-root-time dependence and can be located predominantly within the quantum wells. The process affects all operating points and is manifested by the square-root-shaped shift of the peak emission wavelength. The second degradation mechanism can be attributed to a defect formed quantum well bypass, reducing the carrier population within the quantum wells. The progression of the decay follows a logarithmic time dependence and affects all operating points.

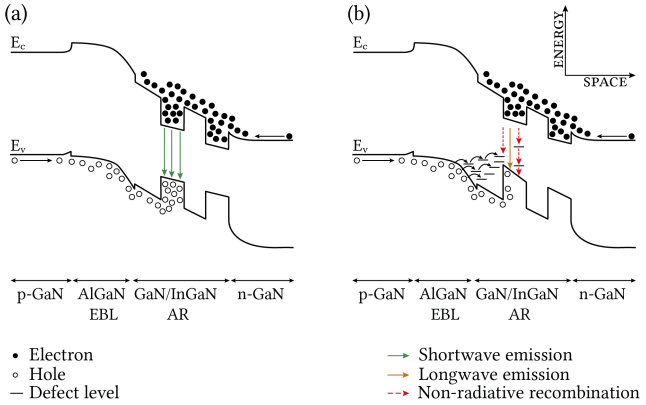

FIGURE 8. Schematic illustration of internal polarization fields at high carrier densities (a.). Reduced QCSE screening by a decreased number of carriers being injected into the quantum well, which results in a spectral red shift (b).

C. POSSIBLE DEFECT ORIGINS

The origin of the generated point defects is variously discussed in the literature. Due to the lower growth temperature of indium-rich layers and the lattice mismatch to neighboring GaN barriers, the active region suffers from a higher defect density with increasing indium concentration [34]. Both the density of native defects and the density of impurities affect the purity of the InGaN crystal and thus the lifetime of the device. Native defects commonly found in GaN devices are nitrogen interstitials, nitrogen vacancies, nitrogen antisite defects, gallium vacancies and gallium interstitials. Defects related to foreign impurities include hydrogen, iron, carbon, magnesium, oxygen, and silicon [36]. Both defect types can contribute to an increase in SRH recombinations and trap-assisted tunneling processes. According to Roccato et al., trap energy levels close to the mid-gap result in a higher TAT probability and in increased SRH recombination rates R_{SRH} [24]. Buffolo et al. stated a highly detrimental contribution of Ga-vacancies (V_{Ga}), due to its potential of hole transport prevention inside the active region, the formation of V_{Ga}-H_n complexes and the release of hydrogen during operation [34]. In addition, the impact of the defects is particularly strong if they are located close to the n-doped region, since the number of electrons injected into the quantum well is reduced as a result. The effect is not less significant if holes cannot be effectively injected into the active region [34].

However, it should be noted that, in general, various defects could be considered as a potential source of the observed radiant flux depreciation, which cannot be specified in more detail without a comprehensive material analysis. Therefore, we propose a feasible literature-based scenario describing the observed degradation characteristics.

Due to the square-root-time dependence of the degradation dynamics and the current state of literature, we suggest diffusion processes to be involved in the formation of the defects [37], [38], [39], [40], [41], [42], [43].

Based on current research results, the initial diffusion process for $t < 200\,\mathrm{h}$ could be caused by altering magnesium or hydrogen concentration profiles [37], [38], [39]. During the manufacturing process, hydrogen is incorporated into the semiconductor as a result of the epitaxial layer growth. Especially in the p-doped region, an increased concentration of hydrogen can be observed, which is strongly correlated to the magnesium doping profile and the passivation of the magnesium acceptors.

Due to the similarities between magnesium and hydrogen concentration profiles, the electron blocking layer shows the highest concentration of hydrogen atoms [37], [44]. While binding of hydrogen atoms to acceptors reduces the conductivity of the p-type region, hydrogen also passivates point defects in the active region, resulting in an increase in radiative recombination processes [37]. Vice versa, the bond breaking of Mg-H complexes during operation has a positive effect on the conductivity of the p-type region [37].

When analyzing the degradation mechanisms of AlGaN emitters, Glaab et al. observed a separation of hydrogen atoms from V_{Ga}-H_n complexes, followed by a concentration gradient that drives hydrogen atoms to diffuse to the n-doped region [37]. The dehydrogenation of passivated point defects with accompanied diffusion of H^+ ions into the n-doped region leaves behind stationary point defects. These point defects are acting as non-radiative recombination centers, thus contributing to a reduced device efficiency. According to literature, the dehydrogenation energy of V_{Ga}-H_n complexes can be quantified with approximately 1 eV - 3.25 eV [45], [46]. Even though the effect has so far only been observed in AlGaN emitters and GaN devices, it remains a reasonable scenario for in InGaN emitters [37], [47].

The removal of H atoms from V_{Ga}-H_n complexes can be induced by various interactions:

a.) Temperature driven effects can be considered in general. At a junction temperature of $T_j = 86\,^{\circ}\mathrm{C}$, the thermal energy can be quantified with 31 meV, which allows us to rule out a primarily temperature-induced dehydrogenation of the defects.

b.) Leung et al., Ruschel et al. and Meneghini et al. reported that the formation of the defects in III-V compound semiconductors can be attributed to the interaction with hot carriers [16], [48], [49]. Hot electrons can arise from AM recombinations, which are particularly detectable in indium-rich quantum well structures due to the distorted band structure [50]. In studies by Iveland et al. [51] a local maximum of hot electrons with a kinetic energy of 2 eV was observed in the energy spectrum of InGaN LEDs. Consequently, it can be assumed that the degradation of high-power green LEDs is additionally enhanced by the comparatively high rate of Auger-Meitner recombination and the associated rate of hot carriers.

c.) In addition, recent studies have identified a novel variant of AM-driven recombination processes, distinct from conventional Auger-Meitner recombination due to its modulation by trap concentration [34], [52], [53], [54]. The process, also known as trap-assisted Auger-Meitner (TAAM) recombination, is characterized by a quadratic dependence with carrier density and a direct correlation with defect density, thus potentially accelerating the degradation of green emitting indium-rich quantum well structures with high defect densities. As this recombination mechanism has only recently been proposed, its effects on radiant flux depreciation have not yet been fully investigated [34].

d.) Finally, the process of photo-induced de-hydrogenation must be considered. In the studies by De Santi et al., a generation of point defects in irradiated InGan LEDs with a 405 nm laser was demonstrated [55], [56]. Due to the previously mentioned dehydrogenation energy between 1 eV - 3.25 eV an interaction with photons could also be considered ($522\,\mathrm{nm} \approx 2.37\,\mathrm{eV}$).

Consequently, the dehydrogenation of V_{Ga}-H_n defect complexes and the subsequent diffusion of hydrogen is a potential explanation for the generation of point defects within the quantum wells [37]. Analogous to the results from Herzog et al. [57], the magnesium back diffusion from the p-doped layers, described by Nam et al. [58], seems unlikely since the effect did not occur at higher current densities in green laser diodes [59].

The second effect of reduced carrier injection can be attributed to a defect increment close to the valence band E_v [34]. According to Park et al. indium-rich InGaN MQWs become unstable at high epitaxial growth temperatures [60]. Therefore, the growth temperature for the subsequently deposited p-type GaN layer is reduced for green LEDs. This limitation in p-type doping results in decreased hole mobility and a lower equilibrium hole concentration compared to blue LEDs [43], [60], [61]. Consequently, an increase in defects with energy levels close to the valence band, causing reduced hole injection into the QW, would exacerbate the prevailing low hole concentration. The reduced carrier concentration in the QW would result in a reduced QCSE screening, thus explaining the observed red shift. According to Buffolo et al., gallium vacancies (V_{Ga}) can be found in indium-rich structures, indicating an energy level close to the valence band E_v [34]. Therefore, these V_{Ga} defects could be a feasible origin for the occurring bypass.

Regarding the electrical characteristics it should be noted, that the series resistance of the device decreases with a

square-root-time dependence, additionally indicating that diffusion processes may be involved. Since Mg acceptors in the p-type region tend to be passivated by hydrogen atoms during the manufacturing process, a subsequent Mg-H bond breaking by temperature or carrier energy results in an increased effective doping level [37], [62]. The separated hydrogen atoms, which are commonly found at interstitial positions, can diffuse through the lattice, leaving behind Mg acceptors that contribute to increased p-type conductivity and thus lower the series resistance of the device.

A more precise localization of the origin of the defects and possible interactions with hot electrons, trap-assisted AM recombinations or photons will be provided based on the data presented in section V.

IV. TEMPERATURE DEPENDENT DEGRADATION

The evaluation of the temperature dependency of the observed degradation mechanisms is based on the data collected at four different junction temperatures with four devices each. At a stress current of $I_a = 700\,\text{mA}$ the junction temperatures were set within the manufacturer's specification and can be quantified with $T_j = 86\,°\text{C}$, $116\,°\text{C}$, $135\,°\text{C}$ and $155\,°\text{C}$.

A. THE EFFECT OF TEMPERATURE ON STRESS TEST RESULTS

Fig. 9 shows the temperature dependent flux depreciation of the emitters at a measurement current of $I_m = 100\,\mu\text{A}$. Within the first 500 hours of operation, the optical power of the different operating temperatures is reduced by approximately 50 %. The initial drop in radiant flux is followed by a decreased degradation rate, further reducing the optical power to 10 % of its initial value. The overall degradation dynamics for the averaged radiant flux of four samples at this operating point can be describes by a logarithmic decay function. Taking into account the deviation of each sample set, no significant difference between the four temperatures can be identified. Furthermore, there is no discernible trend that allows a correlation between the strongest degradation with the highest stress test condition and vice versa.

The peak wavelength shift for 100 µA indicates a blue shift for all stress conditions, shown in Fig. 9. With increasing temperature an increment of the blue shift is observed, thus resulting in a maximum peak wavelength shift of 1.6 nm at $T_j = 155\,°\text{C}$ and a FWHM reduction of $\Delta_{FWHM} = \text{-}0.85\,\text{nm}$. Analogously to the previously described results, a square-root-time dependence can be identified for the different junction temperatures. Defining a peak wavelength shift of $\Delta_{\lambda,peak} = \text{-}0.75\,\text{nm}$ as a failure criterion, an Arrhenius-like temperature dependency of the spectral shift with an activation energy of $E_a = 0.23 \pm 0.025\,\text{eV}$ ($R^2 = 0.98$) can be revealed.

Operating points above the efficiency maximum indicate a different degradation characteristic, representatively shown for 10 mA in Fig. 10. Analogously to the previously presented results, the time dependent radiant flux depreciation

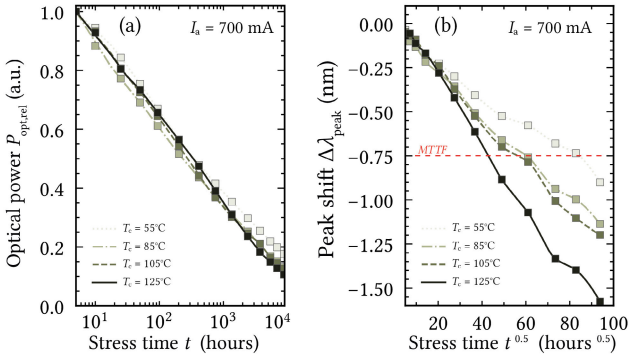

FIGURE 9. Radiant flux depreciation measured at $I_m = 100\,\mu\text{A}$ and a case temperature of $T_c = 25\,°\text{C}$ for a stress current of $I_a = 700\,\text{mA}$ and four different stress test junction temperatures $T_j = 86\,°\text{C}$, $116\,°\text{C}$, $135\,°\text{C}$ and $155\,°\text{C}$, shown with logarithmic time scaling (a.). Peak wavelength shift $\Delta\lambda_{peak}$ at analogous stress and measurement conditions as a function of the square-root of time (b.). Mean values from four samples each.

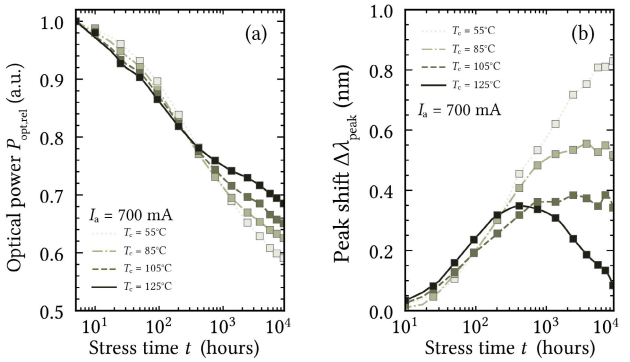

FIGURE 10. Radiant flux depreciation measured at $I_m = 10\,\text{mA}$ and $T_c = 25\,°\text{C}$ for a stress current of $I_a = 700\,\text{mA}$ and four different stress test junction temperatures $T_j = 86\,°\text{C}$, $116\,°\text{C}$, $135\,°\text{C}$ and $155\,°\text{C}$, shown with logarithmic time scaling (a.). Peak wavelength shift $\Delta\lambda_{peak}$ at analogous stress and measurement conditions (b.). Mean values from four samples each.

is separated in two degradation modes. The decay rate in the initial drop (t<200 h) is slightly accelerated by temperature, whereas the subsequent characteristics indicate a slower degradation with higher operating temperature, thus contradicting the findings of previous aging studies [22], [63], [64], [65], [66]. Consequently, the device degradation is less serve with higher operating temperature.

The optical power losses above EQE_{max} are accompanied by colorimetric changes, indicated by red shifts of the measured peak wavelength. For a measurement current of $I_m = 10\,\text{mA}$, the temperature dependent shifts of the peak wavelength are shown in Fig. 10. Within the first 300 hours of operation, the emitters indicate comparable spectral shifts. Subsequently, the junction temperature of $T_s = 55\,°\text{C}$ shows the strongest spectral shift, whereas an increased temperature results in a counteracting blue shift. For a temperature of $T_j = 155\,°\text{C}$, the opposing shift is most prominent, reaching approximately its initial peak wavelength after 9000 hours of

operation. This positive effect of temperature is also prevalent for higher operating points ($I_m > 100$ mA), but as mentioned before, pronounced to a smaller extent.

For an operating point of 200 mA (not shown here) a degradation of 4 % can be observed within the first 1000 hours of operation, subsequently increasing to about 10 % between 1000 and 8800 hours. Due to the standard deviation of the measured data, the effect of temperature on the progression of the degradation mechanisms is only slightly evident. The lower measurement currents exhibit higher sensitivity to the degradation mechanisms, allowing to separate the effect of different junction temperatures for operating points above and below the efficiency maximum.

Electrical parameters extracted from the *I-V* characteristics, such as series resistance R_s or ideality factor n_{ideal} in dependence of stress temperature are not presented in detail. With increasing operating time, the series resistance is reduced independently of temperature by 15 % for all samples with a square-root-time dependence. The square-root-time dependence is also prevalent for the calculated ideality factors. In contrast to the series resistance, higher operating temperatures are accompanied by stronger ascends of ideality factors (15 % at $T_j = 86$ °C and 38 % at $T_j = 155$ °C).

B. DISCUSSION OF TEMPERATURE DRIVEN MECHANISMS

Based on the data of the temperature-dependent degradation, the results from section III-A can be manifested. The decrease of the radiant flux for the operating point of 100 µA is primarily dominated by the logarithmically progressing degradation mechanism, which forms a bypass of the quantum well region. When considering the mean values for the different temperatures shown in Fig. 9, the initial square-root-time dependence is more strongly superimposed by the logarithmic decay compared to the representative LED shown in section III-A. Consequently, the aging mechanism that leads to a bypass of the quantum wells indicates no significant temperature dependence for the considered operating points ($I_m < I_{EQE,max}$). Conversely, the temperature-dependent peak wavelength shifts follow a square-root-time dependence for each aging condition and thus represent analogously to the previous section the degradation process within the quantum wells. It should be noted that there is a linear correlation between peak wavelength shift and ideality factor ($R^2 \approx 0.98$). In this respect, it can be assumed that the ideality factor reflects the degradation processes within the QW, but not the mechanism that can be attributed to a logarithmically progressing reduced carrier injection.

Assuming that the observed spectral blue shift originates from a diffusion process, the temperature dependence of the diffusion constants can be described using the Arrhenius equation. The derived activation energy of $E_a = 0.23 \pm 0.025$ eV is below the previously published values for H diffusion in p-GaN. Nevertheless, taking into account the overview of defect migration barriers in GaN published by Orita et al., the calculated value is consistent with previous studies [42].

TABLE 3. Migration barriers in GaN according to Orita et al. [42].

Defect type	Diffusion type	E_a (eV)	Reference
Magnesium	(through dislocation)	0.28	[68]
Oxygen	(through dislocation)	0.12	[69]
Hydrogen	(in bulk)	0.96	[47]
Interstitial Gallium	(in bulk)	1.99	[70]
Silicon	(in bulk)	1.55	[42]
Magnesium	(in bulk)	1.23	[71]
Nitrogen vacancy	(in bulk)	4.1	[70]

Since migration barriers for bulk materials are significantly higher than the derived activation energy, a diffusion via threading dislocations seems likely. Assuming a constant factor for barrier reduction between bulk material and threading dislocations, a reduced barrier for the diffusion of hydrogen via threading dislocations can be estimated using the ratio between the activation energies of in the bulk material magnesium diffusion and its diffusion via dislocations [42]. This results in a reduced migration barrier of $E_a = 0.22$ eV for the diffusion of hydrogen via threading dislocations. Consequently, this allows us to support our previously constructed hypothesis of V_{Ga}-H_n complex dehydrogenation as a possible origin for defect formation within the quantum wells.

For operating points above EQE_{max}, the degradation dynamics are dominated by the observed bypass mechanism. For (t>200 h), an inverse temperature dependence emerges, which is accompanied by spectral blue shifts counteracting the previously discussed red shift. Due to the persisting logarithmic flux decay with a simultaneous counteracting blue shift of the peak wavelength, it can be assumed that the effect is not due to an improved injection efficiency of holes. If the counteracting blue shift was due to an improved injection efficiency, the almost complete spectral shift compensation at $T_j = 155$ °C and $t = 8800$ h should be accompanied by an increasing radiant flux. Given the fact, that the progressing logarithmic decay indicates a temperature-independent uniform gradient between 5000 and 8800 hours, it seems likely that a third temperature-dependent mechanism is involved in the atypical temperature dependency.

According to Zhang et al., the previously described process can be caused by a compensation of the QCSE by a diffusion of ionized magnesium acceptors [44]. Due to the high dopant concentration in the electron blocking layer and the p-doped region, diffusion of magnesium acceptors into the active region can occur. The internal electric fields caused by the material are compensated by Mg acceptors in the edge region of the quantum wells. The resulting reduced distortion of the band structure results in a blue shift of the emission spectrum and is schematically illustrated in Figure 11.

With increasing temperature, a stronger diffusion of the acceptors can be assumed, thus resulting in a stronger compensation of the QCSE, which is additionally associated

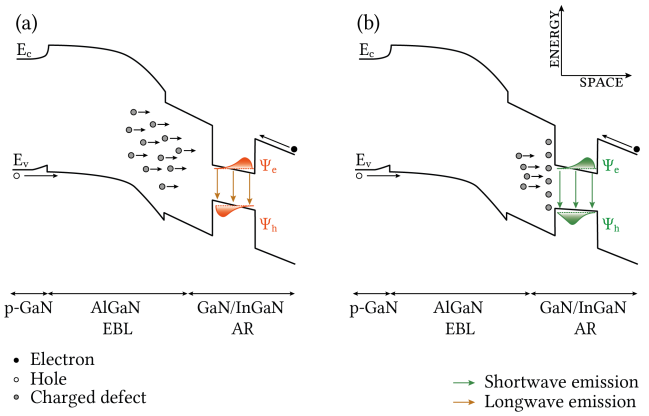

FIGURE 11. Schematic illustration of charged defect diffusion at the beginning of the stress test, with reduced e/h wave function overlap (a.) and after t>200 h with increased QCSE screening and increased e/h wave function overlap, resulting in a spectral blue shift (b).

with an increased overlap of the wave functions and with a higher radiative recombination rate. Considering the results of Strauss et al. [59] and Marona et al. [71], which contradict the scenario of magnesium diffusion in InGaN devices, it can be assumed that the third mechanism is not necessarily limited to the diffusion of magnesium acceptors, but can also be caused by the diffusion of other charged defects.

V. CURRENT DEPENDENT DEGRADATION

Besides the prevailing junction temperature, the current flow through the devices plays a key role in accelerating degradation dynamics. To analyze the effect of the stress current on the radiant flux depreciation, the samples were operated in an isothermal test design at a temperature of $T_j \approx 135\,°C \pm 4\,K$ and three different forward currents. The constant current stress conditions were chosen within the manufacturer's specification and can be quantified with $I_a = 350\,mA$, 700 mA and 1000 mA.

A. THE EFFECT OF FORWARD CURRENT ON STRESS TEST RESULTS

Fig. 12 shows the radiant flux decay for an operating point of $I_m = 100\,\mu A$ at three different stress currents and an aging period of 8800 hours. Analogous to the results from section IV, a significant degradation of the devices can be observed for the entire test period, indicating a logarithmically progressing flux decay. Contrary to the temperature dependent aging results shown in Fig. 9, the degradation behavior differs slightly for the analyzed forward currents.

The device operated at $I_a = 350\,mA$ is subject to a less severe initial degradation persisting as an offset for the overall stress time. Furthermore, no significant difference was found between the radiant flux depreciation at $I_a = 700\,mA$ and 1000 mA.

The observed peak wavelength shifts are also in line with the results from section IV. The corresponding peak wavelength shifts are presented in Fig. 12, slightly deviating

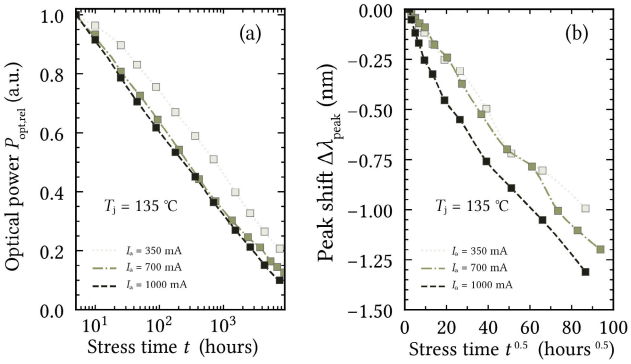

FIGURE 12. Radiant flux depreciation measured at $I_m = 100\,\mu A$ and $T_c = 25\,°C$ for a stress current of $I_a = 350$ mA, 700 mA and 1000 mA at a stress test junction temperature of $T_j = 135\,°C$, shown with logarithmic time scaling (a.). Peak wavelength shift $\Delta\lambda_{peak}$ at analogous stress and measurement conditions as a function of the square-root of time. (b.) Mean values from four samples each.

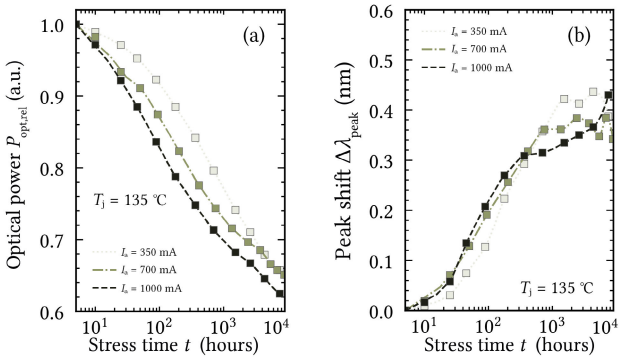

FIGURE 13. Radiant flux depreciation measured at $I_m = 10$ mA and $T_c = 25\,°C$ for a stress current of $I_a = 350$ mA, 700 mA and 1000 mA at a stress test junction temperature of $T_j = 135\,°C$, shown with logarithmic time scaling (a.). Peak wavelength shift $\Delta\lambda_{peak}$ at analogous stress and measurement conditions (b.) Mean values from four samples each.

from an ideal square-root-time dependence ($R^2 = 0.97$). Due to the standard deviation of the results, no significant effect of increased stress current can be manifested.

For operating points above EQE_{max}, representatively shown for $I_m = 350$ mA in Fig. 13, an increase in forward current is accompanied by a significantly reduced time to failure. Due to almost identical junction temperatures, the peak wavelength shifts are progressing uniformly and are counteracted to a similar extent.

The significant differences between the radiant flux depreciations for the analyzed stress currents at $I_m = 10\,mA$ facilitate the analysis of current-induced acceleration of the initial degradation mechanism. To assess the initial degradation process largely independently of subsequent mechanisms, a 10 % reduction in radiant flux is defined as a failure criterion, shown in Fig. 14.

The derived L_{90} lifetimes indicate a shortened time to failure for increasing stress current. The non-thermal acceleration of the degradation processes is commonly

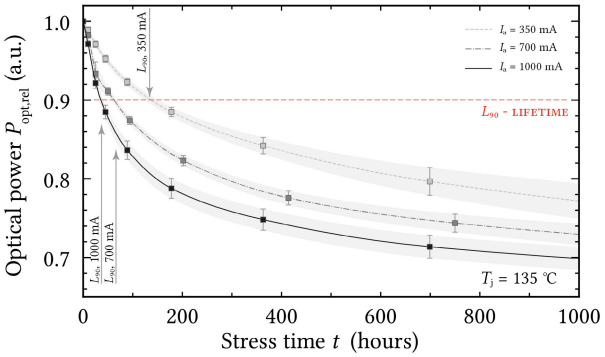

FIGURE 14. Radiant flux depreciation within 1000 hours of operation for the stress current of $I_a = 350$ mA, 700 mA and 1000 mA at $T_j = 135$°C, shown with linear time scaling. The defined L_{90} lifetime criterion is shown in dashed red. Mean values from four samples each with calculated standard deviation (shades), measured at $T_c = 25$°C.

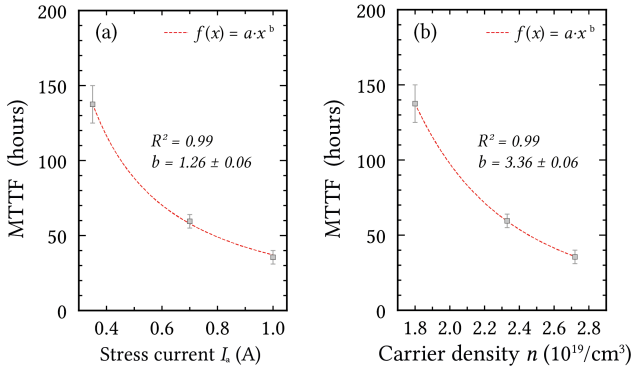

FIGURE 15. Extracted MTTF values for a defined L_{90} lifetime criterion depending on stress current I_a, fitted using an inverse power law function (a.) Analogues procedure for the MTTF values depending on calculated stress test carrier densities n (b.). Mean values from four samples each, measured at $T_c = 25$ °C.

described using an inverse power law [57]. Therefore, the defined lifetime criterion L_x is given as a function of the aging current I_a with the parameter D and the exponent b by

$$L_x = D \cdot I_a^{-b} \tag{2}$$

From the MTTF shown in Fig. 15, the parameters D and b can be determined by least squares regression. The coefficient of determination can be quantified with $R^2 = 0.99$, indicating an appropriate representation of the dependencies. The exponent for the L_{90} lifetimes depending on stress current I_a results in $b_I = 1.26 \pm 0.06$. For a L_{85} criterion the value increases slightly to $b_I = 1.36 \pm 0.16$.

To provide further insight into the underlying degradation mechanisms, the lifetime will be determined as a function of the carrier density n. Assuming that the recombination rate R within the LED is a function of the forward current I_f, the volume of the active region V_{active} and the elementary charge e, given by:

$$R = I_f / eV_{active}. \tag{3}$$

According to Schubert [32], the charge carrier density n can be estimated using the measured absolute spectrum with

$$n = \sqrt{\frac{P_{opt}/(h\nu)}{\eta_{extr}\eta_{inj}V_{active}B}}. \tag{4}$$

The volume of the active region V_{active} is assumed with a chip area of $A_c = 1\,\text{mm}^2$, a quantum well layer thickness of $d_{QW} = 3.5$ nm and a number of $n_{QW} = 5$ quantum wells. Due to the unavailability of manufacturer data, the number and the thickness of quantum wells are based on values from the literature [7]. The number of emitted photons is determined with $P_{opt}/(h\nu)$, using the absolutely measured spectral data, the spectral optical power P_{opt}, Planck's constant h and the photon frequency ν.

The injection efficiency η_{inj} into the previously defined volume V_{active} and the extraction efficiency η_{extr} are taken into account with 100 % and 67.5 % respectively. At this point, it should be noted that the absolute value of b_n does not change for other efficiency values and material parameters since the ratio between the determined stress test carrier densities is not affected. Within the range of adopted stress currents the extraction efficiency and injection efficiency are not expected to vary significantly. Furthermore, we assume that the material parameters for the analyzed devices are approximately identical.

Based on the assumptions made, the shape of external and internal quantum efficiencies are identical. The material-dependent bimolecular recombination coefficient, through which processes of radiative recombination are taken into account, is assumed with $B = 1 \times 10^{-12}\,\text{cm}^3/\text{s}$ [35]. Taking into account equation 4 and the previously described parameters, the lifetime in dependence of carrier density n is given by Fig. 15 (b). Deriving the inverse power law exponent b_n analogously to Fig. 15 (a), the exponent of the inverse power function results in $b_n = 3.36 \pm 0.06$ (L_{85} results in $b_n = 3.6 \pm 0.13$).

B. DISCUSSION OF CURRENT DRIVEN EFFECTS

Analogous to the results of the temperature-dependent stress tests, no significant degradation acceleration arises from an increased stress current for operating points below EQE_{max}. As a result of the logarithmically progressing flux depreciation, it can be assumed that the operating points are primarily dominated by the previously described bypass mechanism. Due to the strong variance of the data, no current-driven acceleration is manifested for the peak wavelength, although its square-root-time dependent progression is consistent with the results of the previous chapter.

For the operating points above EQE_{max}, here in particular for $I_m = 10$ mA, the MTTF of the initial square-root-time-dependent mechanism is accelerated with a negative exponent of $b_n = 3.36 \pm 0.06$ as a function of the carrier density n.

Based on the findings of the previous sections, the degradation of the devices is due to the formation of point defects within the quantum wells. According to Glaab et al.,

the formation of point defects in AlGaN devices could originate from an activation of passivated point defects [37]. The de-hydrogenation of V_{Ga}-H_n complexes can be caused by an interaction with hot electrons [45], [46]. Taking into account the derived exponent $b_n = 3.36 \pm 0.06$ and the proportionality of Auger-Meitner recombinations R_{Auger} with the carrier density

$$R_{Auger} \propto n^3, \tag{5}$$

it can be assumed that the current-induced increase of AM recombinations also affects the degradation of the InGaN green emitters. In line with the results from Ruschel et al. [49], defect formation occurs through a number N_{Auger} of Auger-Meitner processes associated with the generation of hot electrons and a resulting number of reactivated point defects. The number of processes causing a reduction of the optical power to x-percent of the output power is given by aging time L_x and Auger rate R_{Auger} via

$$L_x \cdot R_{Auger} = N_{Auger}. \tag{6}$$

In contrast to the results of Ruschel et al., the cubic acceleration of the degradation is a function of the carrier density, whereas Ruschel et al. derived it as a function of forward current. Based on the cubic acceleration with carrier density, an AM driven defect formation seems likely.

As a result of an indiscernible Arrhenius behavior, the previously discussed scenario of thermally induced defect generation is not primarily affecting the observed degradation dynamics. Furthermore, interactions with photons, which would be accelerated with the square of the carrier density, cannot be manifested based on the presented results. Due to its cubic dependence on carrier density, the degradation cannot be linked to the recently discovered trap-assisted Auger-Meitner recombination process, which is supposed to have a quadratic dependence on the carrier density [34], [52], [53], [54].

Based on these findings, it can be stated that the concentration of the initially generated defects depends in the first instance on the number of interactions with hot electrons. At this point it remains questionable whether the observed degradation is due to a separation of hydrogen from V_{Ga}-H_n complexes by hot electrons, followed by a subsequent diffusion to the n-side during operation, leaving behind negatively charged point defects. Since these mechanisms have only been observed in AlGaN emitters, follow-up experiments on InGaN structures could reveal whether these mechanisms contribute significantly to the device degradation here as well.

VI. CONCLUSION

The degradation of green high-power LEDs, governed primarily by die-intrinsic mechanisms, was investigated through stress tests conducted for up to 8800 hours with forward currents ranging from 350 mA to 1000 mA and junction temperatures between 86 °C and 155 °C. A contribution of package-related mechanisms, including changes in the thermal structure functions, is not manifested based on the presented data. Due to the significant efficiency droop of these indium-rich emitters, the extent of flux depreciation and its temporal progression are not uniform for all operating points. In general, the radiant flux depreciation is driven by the following mechanisms: 1.) The generation of point defects in the active region, reducing the rate of radiative recombination by forming defect levels promoting Shockley-Read-Hall recombination. 2.) The formation of defect levels close to the valence band, reducing the number of injected carriers in the quantum wells, which is accompanied by a spectral red shift for operating points above the efficiency maximum. 3.) A temperature driven diffusion of charged defects to the active region with an activation energy of $E_a = 0.23 \pm 0.025$ eV, which compensates internal polarization fields and leads to an unexpected improvement in device lifetime at elevated temperatures. 4.) The cubic degradation acceleration with carrier density, following $t \propto n^{-3.36}$, suggests an involvement of AM recombination in defect generation. Therefore, the interaction of hot electrons with V_{Ga}-H_n complexes and subsequent hydrogen separation and diffusion, appears to be a plausible explanation for the observed degradation effects. The derived activation energy manifests our hypothesis of hydrogen diffusion involvement. To confirm the described mechanisms, additional characterizations with deep level spectroscopy and secondary-ion mass spectrometry should be carried out in follow-up experiments.

ACKNOWLEDGMENT

The JU receives support from the European Union's Horizon 2020 Research and Innovation Program and The Netherlands, Hungary, France, Poland, Austria, Germany, Italy, and Switzerland. The work reported in this article reflects the author's view and the JU is not responsible for any use that may be made of the information it contains.

REFERENCES

[1] P. Kusuma, P. M. Pattison, and B. Bugbee, "From physics to fixtures to food: Current and potential LED efficacy," *Horticulture Res.*, vol. 7, no. 1, pp. 1–9, Dec. 2020.

[2] M. Meneghini, L.-R. Trevisanello, G. Meneghesso, and E. Zanoni, "A review on the reliability of GaN-based LEDs," *IEEE Trans. Device Mater. Rel.*, vol. 8, no. 2, pp. 323–331, Jun. 2008.

[3] M. Yamada, T. Mitani, Y. Narukawa, S. Shioji, I. Niki, S. Sonobe, K. Deguchi, M. Sano, and T. Mukai, "InGaN-based near-ultraviolet and blue-light-emitting diodes with high external quantum efficiency using a patterned sapphire substrate and a mesh electrode," *Jpn. J. Appl. Phys.*, vol. 41, no. 2, pp. L1431–L1433, Dec. 2002.

[4] N. Renso, M. Meneghini, M. Buffolo, C. De Santi, G. Meneghesso, and E. Zanoni, "Understanding the degradation processes of GaN based LEDs submitted to extremely high current density," *Microelectron. Rel.*, vols. 76–77, pp. 556–560, Sep. 2017.

[5] M. R. Krames, O. B. Shchekin, R. Mueller-Mach, G. O. Mueller, L. Zhou, G. Harbers, and M. G. Craford, "Status and future of high-power light-emitting diodes for solid-state lighting," *J. Display Technol.*, vol. 3, no. 2, pp. 160–175, Jun. 2007.

[6] L.-R. Chen, S.-C. Huang, J.-L. Chiu, C.-C. Lu, W.-M. Su, C.-Y. Weng, H.-Y. Shen, T.-C. Lu, and H. Chen, "Degradation mechanisms of bias stress on nitride-based near-ultraviolet light-emitting diodes in salt water vapor ambient," *Microelectronic Eng.*, vol. 218, Oct. 2019, Art. no. 111158.

[7] I. Titkov, S. Karpov, A. Yadav, D. Mamedov, V. Zerova, and E. Rafailov, "Efficiency of true-green light emitting diodes: Non-uniformity and temperature effects," *Materials*, vol. 10, no. 11, p. 1323, Nov. 2017.

[8] T. Langer, A. Kruse, F. A. Ketzer, A. Schwiegel, L. Hoffmann, H. Jönen, H. Bremers, U. Rossow, and A. Hangleiter, "Origin of the 'green gap' increasing nonradiative recombination in indium-rich GaInN/GaN quantum well structures," *Phys. Status Solidi C*, vol. 8, nos. 7–8, pp. 2170–2172, Jul. 2011.

[9] H. Zhao, G. Liu, J. Zhang, J. D. Poplawsky, V. Dierolf, and N. Tansu, "Approaches for high internal quantum efficiency green InGaN light-emitting diodes with large overlap quantum wells," *Opt. Exp.*, vol. 19, no. S4, pp. A991–A1007, 2011.

[10] F. Nippert, S. Y. Karpov, G. Callsen, B. Galler, T. Kure, C. Nenstiel, M. R. Wagner, M. Straßburg, H.-J. Lugauer, and A. Hoffmann, "Temperature-dependent recombination coefficients in InGaN light-emitting diodes: Hole localization, Auger processes, and the green gap," *Appl. Phys. Lett.*, vol. 109, no. 16, Oct. 2016, Art. no. 161103.

[11] Y. Jiang, Y. Li, Y. Li, Z. Deng, T. Lu, Z. Ma, P. Zuo, L. Dai, L. Wang, H. Jia, W. Wang, J. Zhou, W. Liu, and H. Chen, "Realization of high-luminous-efficiency InGaN light-emitting diodes in the 'green gap' range," *Sci. Rep.*, vol. 5, no. 1, p. 10883, Jun. 2015.

[12] R. Mueller-Mach, G. O. Mueller, T. A. Trottier, M. R. Krames, A. Kim, and D. A. Steigerwald, "Green phosphor-converted LED," *Proc. SPIE*, vol. 4776, pp. 131–136, Nov. 2002.

[13] F. Rahman, A. F. George, and R. Drinkard, "Short-and long-term reliability studies of broadband phosphor-converted red, green, and white light-emitting diodes," *IEEE Trans. Device Mater. Rel.*, vol. 16, no. 1, pp. 1–8, Mar. 2016.

[14] Z. L. Li, P. T. Lai, and H. W. Choi, "A reliability study on green InGaN–GaN light-emitting diodes," *IEEE Photon. Technol. Lett.*, vol. 21, no. 19, pp. 1429–1431, Oct. 1, 2009.

[15] N. Narendran, L. Deng, R. M. Pysar, Y. Gu, and H. Yu, "Performance characteristics of high-power light-emitting diodes," in *Proc. 3rd Int. Conf. Solid State Lighting*, 2004, pp. 267–275.

[16] M. Meneghini, U. Zehnder, B. Hahn, G. Meneghesso, and E. Zanoni, "Degradation of high-brightness green LEDs submitted to reverse electrical stress," *IEEE Electron Device Lett.*, vol. 30, no. 10, pp. 1051–1053, Oct. 2009.

[17] P. Tangyunyong and M. A. Miller, "Characterization of failure modes in deep UV and deep green LEDs utilizing advanced semiconductor localization techniques," Sandia Nat. Lab. (SNL-NM), Albuquerque, NM, USA, Tech. Rep. SAND2012-1853, 2012.

[18] *Approved Method: Measuring Luminous Flux and Color Maintenance of LED Packages, Arrays, and Modules*, Standard IES LM-80-20, Illuminating Engineering Society of North America, New York, NY, USA, 2020.

[19] D. Zhu, J. Xu, A. N. Noemaun, J. K. Kim, E. F. Schubert, M. H. Crawford, and D. D. Koleske, "The origin of the high diode-ideality factors in GaInN/GaN multiple quantum well light-emitting diodes," *Appl. Phys. Lett.*, vol. 94, no. 8, Feb. 2009, Art. no. 081113.

[20] D.-P. Han, C.-H. Oh, H. Kim, J.-I. Shim, K.-S. Kim, and D.-S. Shin, "Conduction mechanisms of leakage currents in InGaN/GaN-based light-emitting diodes," *IEEE Trans. Electron Devices*, vol. 62, no. 2, pp. 587–592, Feb. 2015.

[21] A. Herzog, M. Wagner, and T. Q. Khanh, "Monitoring the optical degradation of green light-emitting diodes on the basis of measured electrical characteristics," *Microelectron. Rel.*, vol. 121, Jun. 2021, Art. no. 114147.

[22] M. Meneghini, M. Dal Lago, N. Trivellin, G. Meneghesso, and E. Zanoni, "Degradation mechanisms of high-power LEDs for lighting applications: An overview," *IEEE Trans. Ind. Appl.*, vol. 50, no. 1, pp. 78–85, Jan. 2014.

[23] A. Herzog, M. Wagner, and T. Q. Khanh, "Efficiency droop in green InGaN/GaN light emitting diodes: Degradation mechanisms and initial characteristics," *Microelectron. Rel.*, vol. 112, Sep. 2020, Art. no. 113792.

[24] N. Roccato, F. Piva, C. D. Santi, R. Brescancin, K. Mukherjee, M. Buffolo, C. Haller, J.-F. Carlin, N. Grandjean, M. Vallone, A. Tibaldi, F. Bertazzi, M. Goano, G. Verzellesi, G. Meneghesso, E. Zanoni, and M. Meneghini, "Modeling the electrical characteristics of InGaN/GaN LED structures based on experimentally-measured defect characteristics," *J. Phys. D, Appl. Phys.*, vol. 54, no. 42, Oct. 2021, Art. no. 425105.

[25] T. Yanagisawa, "Estimation of the degradation of InGaN/AlGaN blue light-emitting diodes," *Microelectron. Rel.*, vol. 37, no. 8, pp. 1239–1241, Aug. 1997.

[26] Z. Peng, Y. Lu, Y. Gao, G. Chen, J. Zheng, Z. Guo, Y. Lin, and Z. Chen, "Effect of carrier localization and Shockley-Read-Hall recombination on the spatial distribution of electroluminescence in InGaN LEDs," *IEEE Photon. J.*, vol. 10, no. 6, pp. 1–8, Dec. 2018.

[27] S. Hafiz, F. Zhang, M. Monavarian, V. Avrutin, H. Morkoç, Ü. Özgür, S. Metzner, F. Bertram, J. Christen, and B. Gil, "Determination of carrier diffusion length in GaN," *J. Appl. Phys.*, vol. 117, no. 1, Jan. 2015, Art. no. 013106.

[28] A. Kaneta, M. Funato, and Y. Kawakami, "Nanoscopic recombination processes in InGaN/GaN quantum wells emitting violet, blue, and green spectra," *Phys. Rev. B, Condens. Matter*, vol. 78, no. 12, Sep. 2008, Art. no. 125317.

[29] C.-K. Li, M. Piccardo, L.-S. Lu, S. Mayboroda, L. Martinelli, J. Peretti, J. S. Speck, C. Weisbuch, M. Filoche, and Y.-R. Wu, "Localization landscape theory of disorder in semiconductors. III. application to carrier transport and recombination in light emitting diodes," *Phys. Rev. B, Condens. Matter*, vol. 95, no. 14, Apr. 2017, Art. no. 144206.

[30] T.-J. Yang, R. Shivaraman, J. S. Speck, and Y.-R. Wu, "The influence of random indium alloy fluctuations in indium gallium nitride quantum wells on the device behavior," *J. Appl. Phys.*, vol. 116, no. 11, Sep. 2014, Art. no. 113104.

[31] Q. Wang, X. Gao, Y. Xu, and J. Leng, "Carrier localization in strong phase-separated InGaN/GaN multiple-quantum-well dual-wavelength LEDs," *J. Alloys Compounds*, vol. 726, pp. 460–465, Dec. 2017.

[32] E. Schubert, *Journal of Alloys and Compounds*, 3rd ed., Elsevier B.V., Amsterdam, The Netherlands, 2018.

[33] M. Meneghini, M. Dal Lago, L. Rodighiero, N. Trivellin, E. Zanoni, and G. Meneghesso, "Reliability issues in GaN-based light-emitting diodes: Effect of DC and PWM stress," *Microelectron. Rel.*, vol. 52, no. 8, pp. 1621–1626, Aug. 2012. [Online]. Available: https://www.sciencedirect.com/science/article/pii/S002627141100477X

[34] M. Buffolo, A. Caria, F. Piva, N. Roccato, C. Casu, C. De Santi, N. Trivellin, G. Meneghesso, E. Zanoni, and M. Meneghini, "Defects and reliability of GaN-based LEDs: Review and perspectives," *Phys. Status Solidi (A)*, vol. 219, no. 8, Apr. 2022, Art. no. 2100727.

[35] S. Karpov, "ABC-model for interpretation of internal quantum efficiency and its droop in III-nitride LEDs: A review," *Opt. Quantum Electron.*, vol. 47, no. 6, pp. 1293–1303, Jun. 2015.

[36] D. Bisi, M. Meneghini, C. de Santi, A. Chini, M. Dammann, P. Brückner, M. Mikulla, G. Meneghesso, and E. Zanoni, "Deep-level characterization in GaN HEMTs-part I: Advantages and limitations of drain current transient measurements," *IEEE Trans. Electron Devices*, vol. 60, no. 10, pp. 3166–3175, Oct. 2013.

[37] J. Glaab, J. Ruschel, T. Kolbe, A. Knauer, J. Rass, H. K. Cho, N. Lobo Ploch, S. Kreutzmann, S. Einfeldt, M. Weyers, and M. Kneissl, "Degradation of (In)AlGaN-based UVB LEDs and migration of hydrogen," *IEEE Photon. Technol. Lett.*, vol. 31, no. 7, pp. 529–532, Apr. 1, 2019.

[38] J. Glaab, C. Ploch, R. Kelz, C. Stölmacker, M. Lapeyrade, N. L. Ploch, J. Rass, T. Kolbe, S. Einfeldt, F. Mehnke, C. Kuhn, T. Wernicke, M. Weyers, and M. Kneissl, "Degradation of (InAlGa)N-based UV-B light emitting diodes stressed by current and temperature," *J. Appl. Phys.*, vol. 118, no. 9, Sep. 2015, Art. no. 113104.

[39] N. Renso, C. De Santi, A. Caria, F. Dalla Torre, L. Zecchin, G. Meneghesso, E. Zanoni, and M. Meneghini, "Degradation of InGaN-based LEDs: Demonstration of a recombination-dependent defect-generation process," *J. Appl. Phys.*, vol. 127, no. 18, May 2020, Art. no. 185701.

[40] C. De Santi, M. Meneghini, G. Meneghesso, and E. Zanoni, "Degradation of InGaN laser diodes caused by temperature- and current-driven diffusion processes," *Microelectron. Rel.*, vol. 64, pp. 623–626, Sep. 2016.

[41] C. H. Seager, S. M. Myers, A. F. Wright, D. D. Koleske, and A. A. Allerman, "Drift, diffusion, and trapping of hydrogen in p-type GaN," *J. Appl. Phys.*, vol. 92, no. 12, pp. 7246–7252, Dec. 2002.

[42] K. Orita, M. Meneghini, H. Ohno, N. Trivellin, N. Ikedo, S. Takigawa, M. Yuri, T. Tanaka, E. Zanoni, and G. Meneghesso, "Analysis of diffusion-related gradual degradation of InGaN-based laser diodes," *IEEE J. Quantum Electron.*, vol. 48, no. 9, pp. 1169–1176, Sep. 2012.

[43] I. S. Romanov, I. A. Prudaev, A. A. Marmalyuk, V. A. Kureshov, D. R. Sabitov, and A. V. Zalov, "Effect of magnesium diffusion into the active region of LED structures with InGaN/GaN quantum wells on internal quantum efficiency," *Russian Phys. J.*, vol. 57, no. 4, pp. 533–535, Aug. 2014.

[44] N. Zhang, X.-C. Wei, K.-Y. Lu, L.-S. Feng, J. Yang, B. Xue, Z. Liu, J.-M. Li, and J.-X. Wang, "Effect of back diffusion of mg dopants on optoelectronic properties of InGaN-based green light-emitting diodes," *Chin. Phys. Lett.*, vol. 33, no. 11, Nov. 2016, Art. no. 117302.

[45] H. Nykänen, S. Suihkonen, L. Kilanski, M. Sopanen, and F. Tuomisto, "Low energy electron beam induced vacancy activation in GaN," *Appl. Phys. Lett.*, vol. 100, no. 12, Mar. 2012, Art. no. 122105.

[46] C. G. Van de Walle, "Interactions of hydrogen with native defects in GaN," *Phys. Rev. B, Condens. Matter*, vol. 56, no. 16, pp. R10020–R10023, Oct. 1997.

[47] Y. S. Puzyrev, T. Roy, M. Beck, B. R. Tuttle, R. D. Schrimpf, D. M. Fleetwood, and S. T. Pantelides, "Dehydrogenation of defects and hot-electron degradation in GaN high-electron-mobility transistors," *J. Appl. Phys.*, vol. 109, no. 3, Feb. 2011, Art. no. 034501.

[48] K. K. Leung, W. K. Fong, P. K. L. Chan, and C. Surya, "Physical mechanisms for hot-electron degradation in GaN light-emitting diodes," *J. Appl. Phys.*, vol. 107, no. 7, Apr. 2010, Art. no. 073103.

[49] J. Ruschel, J. Glaab, B. Beidoun, N. L. Ploch, J. Rass, T. Kolbe, A. Knauer, M. Weyers, S. Einfeldt, and M. Kneissl, "Current-induced degradation and lifetime prediction of 310 nm ultraviolet light-emitting diodes," *Photon. Res.*, vol. 7, no. 7, pp. B36–B40, 2019.

[50] T. Sadi, P. Kivisaari, J. Oksanen, and J. Tulkki, "On the correlation of the Auger generated hot electron emission and efficiency droop in III-N light-emitting diodes," *Appl. Phys. Lett.*, vol. 105, no. 9, Sep. 2014, Art. no. 091106.

[51] J. Iveland, L. Martinelli, J. Peretti, J. S. Speck, and C. Weisbuch, "Direct measurement of Auger electrons emitted from a semiconductor light-emitting diode under electrical injection: Identification of the dominant mechanism for efficiency droop," *Phys. Rev. Lett.*, vol. 110, no. 17, Apr. 2013, Art. no. 177406.

[52] A. C. Espenlaub, D. J. Myers, E. C. Young, S. Marcinkevičius, C. Weisbuch, and J. S. Speck, "Evidence of trap-assisted Auger recombination in low radiative efficiency MBE-grown III-nitride LEDs," *J. Appl. Phys.*, vol. 126, no. 18, Nov. 2019, Art. no. 184502.

[53] A. David, N. G. Young, C. A. Hurni, and M. D. Craven, "Quantum efficiency of III-nitride emitters: Evidence for defect-assisted nonradiative recombination and its effect on the green gap," *Phys. Rev. Appl.*, vol. 11, no. 3, Mar. 2019, Art. no. 031001.

[54] W. Liu, C. Haller, Y. Chen, T. Weatherley, J.-F. Carlin, G. Jacopin, R. Butté, and N. Grandjean, "Impact of defects on Auger recombination in c-plane InGaN/GaN single quantum well in the efficiency droop regime," *Appl. Phys. Lett.*, vol. 116, no. 22, Jun. 2020, Art. no. 222106.

[55] C. De Santi, A. Caria, N. Renso, E. Dogmus, M. Zegaoui, F. Medjdoub, G. Meneghesso, E. Zanoni, and M. Meneghini, "Evidence of optically induced degradation in gallium nitride optoelectronic devices," *Appl. Phys. Exp.*, vol. 11, no. 11, Nov. 2018, Art. no. 111002.

[56] A. Caria, C. De Santi, M. Buffolo, G. Meneghesso, E. Zanoni, and M. Meneghini, "Photon-induced degradation of InGaN-based LED in open-circuit conditions investigated by steady-state photocapacitance and photoluminescence," *J. Appl. Phys.*, vol. 131, no. 4, Jan. 2022, Art. no. 043102.

[57] A. Herzog, S. Benkner, B. Zandi, M. Buffolo, W. D. Van Driel, M. Meneghini, and T. Q. Khanh, "Lifetime prediction of current-and temperature-induced degradation in silicone-encapsulated 365 nm high-power light-emitting diodes," *IEEE Access*, vol. 11, pp. 19928–19940, 2023.

[58] O. H. Nam, K. H. Ha, J. S. Kwak, S. N. Lee, K. K. Choi, T. H. Chang, S. H. Chae, W. S. Lee, Y. J. Sung, H. S. Paek, J. H. Chae, T. Sakong, J. K. Son, H. Y. Ryu, Y. H. Kim, and Y. Park, "Characteristics of GaN-based laser diodes for post-DVD applications," *Phys. Status Solidi (A)*, vol. 201, no. 12, pp. 2717–2720, Sep. 2004.

[59] U. Strauss, T. Lermer, J. Müller, T. Hager, G. Brüderl, A. Avramescu, A. Lell, and C. Eichler, "Study of defects and lifetime of green InGaN laser diodes," *Phys. Status Solidi (A)*, vol. 209, no. 3, pp. 481–486, Mar. 2012.

[60] J. H. Park, J. Cho, E. F. Schubert, and J. K. Kim, "The effect of imbalanced carrier transport on the efficiency droop in GaInN-based blue and green light-emitting diodes," *Energies*, vol. 10, no. 9, p. 1277, Aug. 2017.

[61] M.-S. Oh, M.-K. Kwon, I.-K. Park, S.-H. Baek, S.-J. Park, S. H. Lee, and J. J. Jung, "Improvement of green LED by growing p-GaN on $In_{0.25}GaN$/GaN MQWs at low temperature," *J. Cryst. Growth*, vol. 289, no. 1, pp. 107–112, Mar. 2006.

[62] C.-C. Liu, Y.-H. Chen, M.-P. Houng, Y.-H. Wang, Y.-K. Su, W.-B. Chen, and S.-M. Chen, "Improved light-output power of GaN LEDs by selective region activation," *IEEE Photon. Technol. Lett.*, vol. 16, no. 6, pp. 1444–1446, Jun. 2004.

[63] M. Wagner, A. Herzog, H. Ganev, and T. Q. Khanh, "Led aging acceleration—An analysis from measuring and aging data of 14,000 hours led degradation," in *Proc. 12th China Int. Forum Solid State Lighting (SSLCHINA)*, Apr. 2015, pp. 75–78.

[64] M. Wagner, A. Herzog, H. Ganev, and T. Khanh, "Lifetime calculation of white HP-LEDs from 16,000 hours aging data," *LED Prof. Rev.*, vol. 59, pp. 34–38, Mar. 2017.

[65] M. Meneghini, M. Dal Lago, N. Trivellin, G. Mura, M. Vanzi, G. Meneghesso, and E. Zanoni, "Chip and package-related degradation of high power white LEDs," *Microelectron. Rel.*, vol. 52, no. 5, pp. 804–812, May 2012.

[66] A. Herzog, M. Wagner, S. Benkner, B. Zandi, W. D. van Driel, and T. Q. Khanh, "Long-term temperature-dependent degradation of 175 W chip-on-board LED modules," *IEEE Trans. Electron Devices*, vol. 69, no. 12, pp. 6830–6836, Dec. 2022.

[67] J. Neugebauer and C. G. Van de Walle, "Hydrogen in GaN: Novel aspects of a common impurity," *Phys. Rev. Lett.*, vol. 75, no. 24, pp. 4452–4455, Dec. 1995.

[68] R. R. Wixom and A. F. Wright, "H enhancement of N vacancy migration in GaN," *Appl. Phys. Lett.*, vol. 87, no. 20, Nov. 2005, Art. no. 201901.

[69] S. M. Myers and A. F. Wright, "Theoretical description of H behavior in GaN p-n junctions," *J. Appl. Phys.*, vol. 90, no. 11, pp. 5612–5622, Dec. 2001.

[70] K. Orita, M. Kawaguchi, Y. Kawaguchi, S. Takigawa, and D. Ueda, "Efficient outdiffusion of hydrogen from Mg-doped nitrides by NF_3 annealing," *J. Electron. Mater.*, vol. 38, no. 4, pp. 538–544, Apr. 2009.

[71] L. Marona, P. Perlin, R. Czernecki, M. Leszczyński, M. Boćkowski, R. Jakiela, T. Suski, and S. Najda, "Secondary ions mass spectroscopy measurements of dopant impurities in highly stressed InGaN laser diodes," *Appl. Phys. Lett.*, vol. 98, no. 24, Jun. 2011, Art. no. 241115.

ALEXANDER HERZOG (Senior Member, IEEE) received the B.Sc., M.Sc., and Ph.D. degrees in electrical engineering from Technische Universit´at Darmstadt, in 2012, 2015, and 2020, respectively. Currently, he is a Postdoctoral Researcher and a Research Group Leader with the Laboratory of Adaptive Lighting Systems and Visual Processing, Technische Universit´at Darmstadt. His research interests include lifetime prediction, reliability analysis, digital twins of light-emitting diodes, temporal light artifacts, and visual neurostimulation.

MATTEO BUFFOLO (Senior Member, IEEE) received the master's degree in electronic engineering from the University of Padova, in 2014, and the Ph.D. degree from the Department of Information Engineering, University of Padova, in March 2018. He is currently an Assistant Professor with the University of Padova. His research interests include the reliability of lighting systems employing GaN-based devices (lasers and LEDs) and the investigation of the degradation mechanisms that affect IR laser sources for integrated telecommunication applications.

FRANCESCO PIVA received the Ph.D. degree, in March 2022. His Ph.D. thesis was on the study of the degradation mechanisms of AlGaN-based UV-C LEDs. He is currently an Associate Researcher with the Department of Information Engineering, University of Padova. His research interests include the characterization and modeling of III-V-based LEDs with emitting wavelengths from far UV-C to NIR, with a focus on the investigation of the physical processes responsible for device degradation.

SIMON BENKNER received the B.Sc., M.Sc., and Ph.D. degrees in electrical engineering from Technische Universität Darmstadt, Germany, in 2015, 2017, and 2023, respectively. Currently, he is an Academic Lecturer and also works as a Developer and a Consultant for electronic circuits. Additionally, his work explores advancements in smart electronics and the Internet of Things (IoT). His research interests include the reliability of electronic systems, with a particular emphasis on LED technologies and degradation modeling.

BABAK ZANDI received the M.Sc. and Ph.D. degrees in electrical engineering and information technology from Technische Universität Darmstadt. He was a Research Group Leader at the Laboratory of Adaptive Lighting Systems and Visual Processing, Darmstadt. Currently, he is an AI Expert with the Banking Sector, with a focus on transformer-based large language models, and a Lecturer with Technische Universität Darmstadt. His research interests include the integration of neural networks in heuristic optimization algorithms and the modeling of time-series data. He served as an Editorial Board Member for *Scientific Reports*.

JENS BALASUS received the B.Sc., M.Sc., and Ph.D. degrees in electrical engineering from Technische Universität Darmstadt, in 2017, 2019, and 2024, respectively. He is currently a Postdoctoral Researcher with the Laboratory of Adaptive Lighting Systems and Visual Processing, Technische Universität Darmstadt. His research interests include the optimization of horticultural lighting through virtual plant simulations, horticultural lighting systems, light simulation, optical property measurements, and the use of non-SQL databases.

PAUL MYLAND received the B.Sc. and M.S. degrees in electrical engineering and information technology from Technische Universität Darmstadt, Germany, in 2016 and 2019, respectively, and the Ph.D. degree, in 2024. Since then, he has been a Research Assistant at the Laboratory of Adaptive Lighting Systems and Visual Processing. His current work focuses on the applications of spectral sensors and miniature spectrometers in lighting control. His research interests include color and lighting quality, color perception, museum lighting, and multidimensional lighting optimization.

FELIX WIRTH received the B.A. degree in business administration in Frankfurt, in 2014, and the B.Sc. and M.Sc. degrees in electrical engineering and information technology from Technische Universität Darmstadt, Germany, in 2019 and 2022, respectively, where he is currently pursuing the Ph.D. degree with the Laboratory of Adaptive Lighting Systems and Visual Processing, under the supervision of Prof. Tran Quoc Khanh. Since 2022, he has been a Research Associate at the Laboratory of Adaptive Lighting Systems and Visual Processing, Technische Universität Darmstadt. His research interests include spectral analysis for remote sensing in applied agricultural technologies, the influence of LED lighting on plant growth and biochemical composition, and digital plant phenotyping using computer vision techniques. His expertise includes horticultural lighting, computer vision, deep learning algorithms, Python programming, and MongoDB databases.

WILLEM D. VAN DRIEL received the Graduate degree in mechanical engineering from Eindhoven University of Technology and the Ph.D. degree from Delft University of Technology, The Netherlands. He has more than 25 years of track record in the reliability domain. He is currently a Fellow Scientist with Signify (formerly Philips Lighting). He is also a Professor with Delft University of Technology. His application areas range from healthcare, gas and oil exploration, and semiconductors. He has authored and co-authored more than 350 scientific publications, including journals and conference papers, books or book chapters, and invited keynote lectures. His research interests include solid state lighting, microelectronics and microsystems technologies, virtual prototyping, virtual reliability qualification, and designing for reliability of microelectronics and microsystems. He is the Chair of the Organizing Committee of the IEEE Conference EuroSimE.

MATTEO MENEGHINI (Fellow, IEEE) received the master's and Ph.D. degrees in information engineering (the optimization of GaN-based LED and laser structures) from the University of Padova, Padua, Italy, in 2004 and 2008, respectively. He is currently a Full Professor with the Department of Information Engineering, University of Padova, where he is involved in the electro-optical characterization and modeling of the performance and reliability of LEDs, lasers, HEMTs, and advanced solar.

TRAN QUOC KHANH received the Dr.-Ing. degree in physics and technology of electronic components and the Habilitation degree in mechanical engineering and technical optics from the Institute for Lighting Technology, Technische Universität Ilmenau, Germany, in 1989 and 2005, respectively. Since 2006, he has been a Full Professor and the Head of the Laboratory of Adaptive Lighting Systems and Visual Processing, Technische Universität Darmstadt, where he has been the Dean of the Department of Electrical Engineering and Information Technology, since 2018. He leads research groups in the field of automotive lighting, human-centric lighting, smart indoor lighting, and LED technology.